

Spatial Imputation Drives Cross-Domain Alignment for EEG Classification

Hongjun Liu

School of Intelligence Science and
Technology
University of Science and Technology
Beijing
Beijing, China
D202210386@xs.ustb.edu.cn

Chao Yao*

School of Computer and
Communication Engineering
University of Science and Technology
Beijing
Beijing, China
yaochao@ustb.edu.cn

Yalan Zhang

School of Intelligence Science and
Technology
University of Science and Technology
Beijing
Beijing, China
zhangyl@ustb.edu.cn

Xiaokun Wang

School of Intelligence Science and
Technology
University of Science and Technology
Beijing
Beijing, China
wangxiaokun@ustb.edu.cn

Xiaojuan Ban*

School of Intelligence Science and
Technology
University of Science and Technology
Beijing
Beijing, China
banxj@ustb.edu.cn

Abstract

Electroencephalogram (EEG) signal classification faces significant challenges due to data distribution shifts caused by heterogeneous electrode configurations, acquisition protocols, and hardware discrepancies across domains. This paper introduces IMAC, a novel channel-dependent mask and imputation self-supervised framework that formulates the alignment of cross-domain EEG data shifts as a spatial time series imputation task. To address heterogeneous electrode configurations in cross-domain scenarios, IMAC first standardizes different electrode layouts using a 3D-to-2D positional unification mapping strategy, establishing unified spatial representations. Unlike previous mask-based self-supervised representation learning methods, IMAC introduces spatio-temporal signal alignment. This involves constructing a channel-dependent mask and reconstruction task framed as a low-to-high resolution EEG spatial imputation problem. Consequently, this approach simulates cross-domain variations such as channel omissions and temporal instabilities, thus enabling the model to leverage the proposed imputer for robust signal alignment during inference. Furthermore, IMAC incorporates a disentangled structure that separately models the temporal and spatial information of the EEG signals separately, reducing computational complexity while enhancing flexibility and adaptability. Comprehensive evaluations across 10 publicly available EEG datasets demonstrate IMAC's superior performance, achieving state-of-the-art classification accuracy in both cross-subject and

cross-center validation scenarios. Notably, IMAC shows strong robustness under both simulated and real-world distribution shifts, surpassing baseline methods by up to 35% in integrity scores while maintaining consistent classification accuracy.

CCS Concepts

- Computing methodologies → Neural networks;
- Human-centered computing → Ubiquitous and mobile computing systems and tools.

Keywords

EEG Signal Imputation; EEG Classification; Brain-Computer Interface; Domain Adaptation

1 Introduction

Noninvasive electroencephalography (EEG) is a type of multichannel signal that reflects neural activity and latent psychological states, collected from electrodes deployed on the human scalp. Effective classification of EEG signals is crucial for the development of brain-computer interfaces (BCI) with applications in rehabilitation [10], emotion recognition [5], motor imagery [6], and the diagnosis and monitoring of neurological disorders [38]. However, EEG classifiers often fail in real-world deployment settings due to dataset or distribution shifts, including variations in sensor location configuration, non-uniform electrode distribution, and the dynamic nature of the data [40][22]. As shown in Figure 1, these shifts are common causes of domain gaps in both cross-center and cross-subject scenarios [33]. Consequently, achieving consistent classification performance across both cross-subject and cross-center EEG data shifts remains a primary challenge for EEG classification.

Traditionally, numerous studies have explored transfer learning to address domain gaps, with the assumption that a large amount of unlabeled data or a small amount of labeled data from the target subjects is available [27]. These methods generally fall into two

*Corresponding authors

Permission to make digital or hard copies of all or part of this work for personal or classroom use is granted without fee provided that copies are not made or distributed for profit or commercial advantage and that copies bear this notice and the full citation on the first page. Copyrights for components of this work owned by others than the author(s) must be honored. Abstracting with credit is permitted. To copy otherwise, or republish, to post on servers or to redistribute to lists, requires prior specific permission and/or a fee. Request permissions from permissions@acm.org.

MM '25, Dublin, Ireland.

© 2025 Copyright held by the owner/author(s). Publication rights licensed to ACM.
ACM ISBN 979-8-4007-2035-2/2025/10
<https://doi.org/10.1145/3746027.3755582>

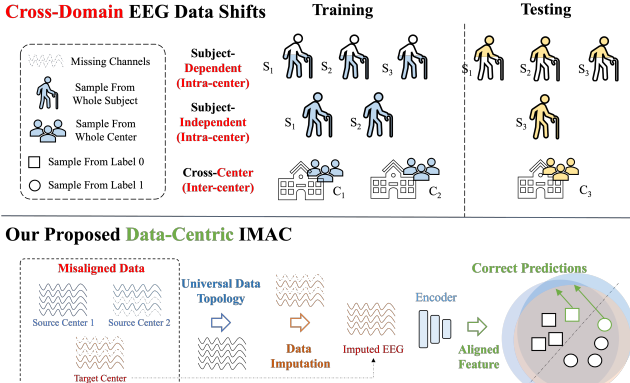


Figure 1: Cross-domain data shifts in real-world setups. In the subject-dependent setup, samples from the same subject can appear in both the training and test sets, causing information leakage. In a subject-independent setup, samples from the same subject are exclusively in either the training or test set, which is more challenging and practically meaningful but less studied. The proposed IMAC aims to perform a cross-domain signal alignment via spatial mask and imputation.

categories: the first compares source and target domain distributions simultaneously, enabling the model to learn domain-invariant features [25][21]; the second uses a source-free mode, where the model is pre-trained on source domain data and then fine-tuned on a large amount of unlabeled data or a small amount of labeled data from the target domain [22][41].

However, when the target subjects are entirely unseen during training, the model must be trained solely on source domain data to create a domain-invariant model. Under this scenario, domain generalization (DG) approaches aim to enable the model to generalize across unseen target domains without requiring additional training data [36]. These approaches can be broadly categorized into feature-based methods and metric-based methods. Feature-based methods, such as data augmentation, domain adversarial training, and domain alignment, focus on learning domain-invariant features. For instance, data augmentation generates synthetic samples to simulate potential domain shifts [39], while domain adversarial training encourages the model to extract features that are indistinguishable across domains [9]. Metric-based methods, in contrast, learn a domain-agnostic metric space where data from different domains are mapped into similar representations [16]. Techniques like prototypical networks aim to align domains by learning this shared metric space [20].

While these methods address domain shifts by training models to learn shared features across domains, they encounter significant limitations under conditions of pronounced heterogeneity [17][35]. These limitations stem from their primary focus on learning domain-invariant features or aligning data distributions across domains without directly addressing the underlying causes of signal discrepancies. In contrast, modifying or correcting the data itself between domains would resolve the domain adaptation problem, rather than merely mitigating their effects through feature learning [40].

To address the data shift challenges specific to EEG classification, in this paper, we tackle data distribution misalignment through spatial time series imputation. We introduce a universal imputation framework called IMpute And Classify (IMAC). The core innovation of IMAC lies in its channel masking and spatial imputation self-supervised learning strategy, which simulates diverse real-world data shifts to effectively bridge cross-domain discrepancies. Specifically, we begin by employing spatial topology unification to standardize the electrode configuration projected into a unified 2D spatial representation. We then apply random channel masking and perform imputation using contextual information, enabling the model to learn cross-domain correlations through a combination of consistency and fidelity losses. This process simulates cross-domain variations and promotes alignment in both spatial and temporal dimensions. Furthermore, we propose a temporal pattern decomposition strategy, which exploits temporal structures from multiple source domains to reduce the complexity of the spatial imputation task while improving computational efficiency. Experiments conducted across 10 public EEG datasets demonstrate that under both simulated and real-world domain shifts, IMAC surpasses baseline methods by up to 35% in integrity scores while preserving consistent EEG classification accuracy, validating its ability to maintain performance stability under heterogeneous recording conditions. The primary contributions of this work can be summarized as follows.

- We formulate the issue of real-world data shifts as a spatial imputation problem. To the best of our knowledge, this is the first work to address cross-domain discrepancies by focusing on signal alignment rather than traditional feature alignment approaches.
- We propose a Temporal-Spatial Decomposition Module that disentangles EEG signals into independent temporal and spatial components. By incorporating a temporal component matching strategy, the model adaptively captures relevant temporal patterns while learning spatial correlations across channels.
- We propose a Channel-dependent Mask and Imputation Module that employs adaptive channel masking to simulate cross-domain variations, leveraging a self-supervised learning strategy to infer complete spatial relationships and reconstruct spatio-temporal signal omissions through a hybrid loss combining consistency and fidelity constraints.

2 Related Works

2.1 Domain Generalization

Domain Generalization aims to improve the model's generalization performance on inaccessible test domains utilizing a series of source domains. The current DG methods can be generally divided into three categories: 1) Domain-invariant feature learning, i.e., learning invariant representations on source domains by adding regularization terms. The author of [9] introduced a multi-view spatial-temporal graph convolutional network (MSTGCN) with domain generalization to address challenges in sleep stage classification by utilizing spatial-temporal features from multi-channel brain signals and improving model generalization across subjects.

2) Data manipulation. The author of [16] proposed a novel domain-generalized EEG classification framework named FDCL to improve the generalizability of EEG decoding methods in unseen subjects by integrating feature decorrelation, data augmentation, and consistency learning regularizations. Study [39] proposed the Denoising Mixed Mutual Reconstruction (DMMR) model to enhance the generalization of EEG-based emotion analysis across subjects through a two-stage pre-training and fine-tuning approach, incorporating self-supervised learning, data augmentation, and noise injection methods. 3) Learning strategies. The author of [20] propose a novel multiscale convolutional prototype network (MCPNet) for automated Parkinson's disease detection using EEG, integrating multi-scale CNN and prototype learning to enhance feature diversity and improve generalization performance. In this work, we introduce a novel data manipulation technique that employs spatial masking and interpolation to achieve direct signal-level alignment, thereby fundamentally reducing distributional discrepancies.

2.2 EEG Spatial Imputation

Super-resolution, initially introduced in image processing, has been widely applied to tasks involving resolution reconstruction in images and videos [11][18][28][29]. Inspired by these advancements, super-resolution techniques have also been adopted and developed for EEG signal processing to address the high cost of high-density EEG devices, named EEG spatial Imputation. Researchers [19] and [3] proposed interpolation-based methods to generate data for additional EEG signal channels. To address the limited effectiveness in multichannel scenarios, the author of [30] introduced a deep EEG super-resolution framework called Deep-EEGSR, which employs sample-specific dynamic convolutions to adapt filter parameters based on individual functional connectivity patterns. Building on this concept, the author of [37] proposed a spatio-temporal adaptive diffusion model (STAD) that enhances the spatial resolution of low-density EEG data using diffusion models and multi-scale Transformer denoising modules. To address the issue of EEG channel selection methods establish a unified paradigm for EEG acquisition devices, ESTformer [15] propose a multihead self-attention mechanism to the space and time dimensions, which can learn spatial structural correlations and temporal functional variations. However, the aforementioned methods did not address three critical issues: real-world EEG variability may arise due to diverse physiological states during acquisition, recording conditions and protocols, and internals of the EEG hardware used.

3 Methods

The overall framework of the proposed method is illustrated in Figure 2. For cross-domain alignment, we begin by employing spatial topology unification to standardize the electrode configurations. With the EEG signals standardized, the proposed Temporal-Spatial Decomposition Module (TSDM) isolates the temporal dynamics and models the channel information separately, facilitating spatial imputation. Lastly, the Channel-dependent Mask and Imputation Module (CMIM) is designed to enable cross-domain knowledge transfer and achieve spatial EEG signal alignment effectively.

3.1 Spatial Topology Unification Module

The proposed Spatial Topology Unification Module (STUM) addresses the challenge of variable channel selection by unifying the spatial topology of EEG signals across multiple datasets. To achieve this, we first define the electrode coordinates based on the widely adopted 10-20 system [8], which provides standardized electrode positions on the scalp. Specifically, the normalized coordinates x_{norm} and y_{norm} for each electrode are scaled and rounded to the nearest integer, thereby mapping them onto a 9×10 matrix. In this matrix, each electrode is assigned a position corresponding to its relative location on the scalp. The matrix is then populated with the EEG signal values, offering a 2D spatial representation of the electrode distribution. However, due to variations in channel configurations across datasets, some electrodes may be missing in certain setups. To address this issue, we apply radial basis function (RBF) interpolation to estimate the missing channels. As a result, we obtain a unified 64-channel spatial topology, ensuring consistency across all datasets.

Following spatial interpolation, we perform cross-channel patching, treating each patch as the unit for subsequent decomposition and spatial imputation. Given an input EEG sample $x_{\text{in}} \in \mathbb{R}^{T \times C}$, we partition it into N non-overlapping cross-channel patches $x^{(p)} = \{x_1^{(p)}, \dots, x_N^{(p)}\}$, where each patch $x_i^{(p)} \in \mathbb{R}^{N \times (L \cdot C)}$, with T representing the number of time steps, C the number of channels, and N the number of patches needed to cover the entire input signal. Finally, for each patch $x_i^{(p)}$, we add a positional embedding feature corresponding to its position, resulting in the set of EEG patches $\hat{x}^{(p)} = \{\hat{x}_1^{(p)}, \dots, \hat{x}_l^{(p)}\}$.

3.2 Temporal-Spatial Decomposition Module

To tackle the challenge of spatio-temporal imputation in EEG data, our IMAC framework aims to recover complete spatial relationships across EEG channels. However, due to the strong coupling between temporal dynamics and spatial distributions in EEG signals, direct spatial reconstruction is particularly difficult [32].

To address this, we propose a Temporal-Spatial Decomposition Module that decouples EEG signals into separate temporal and spatial components, allowing the model to learn temporal dynamics and spatial structures independently. In this module, temporal patterns are encoded as learnable global embeddings Z , while spatial correlations are captured by a channel-dependent matrix $H \in \mathbb{R}^{n \times d}$, where n is the number of channels and d is the embedding dimension.

Given the non-stationary nature of EEG signals, which often exhibit distributional shifts across time and domains, we design a temporal pattern pool that contains pre-learned embeddings representing three fundamental temporal components: trend, seasonality, and residuals. Each component is represented as a fixed embedding Z^T , Z^S , and $Z^R \in \mathbb{R}^{D \times L}$, where D is the temporal feature dimension and L is the length of the time series segment. These embeddings act as reusable bases that encode different types of temporal behavior, enabling adaptive temporal modeling.

To dynamically select the most relevant temporal pattern for a given input patch $\hat{x}^{(p)}$, we introduce a temporal selection function $S(\cdot)$, which computes the cosine similarity between the input and

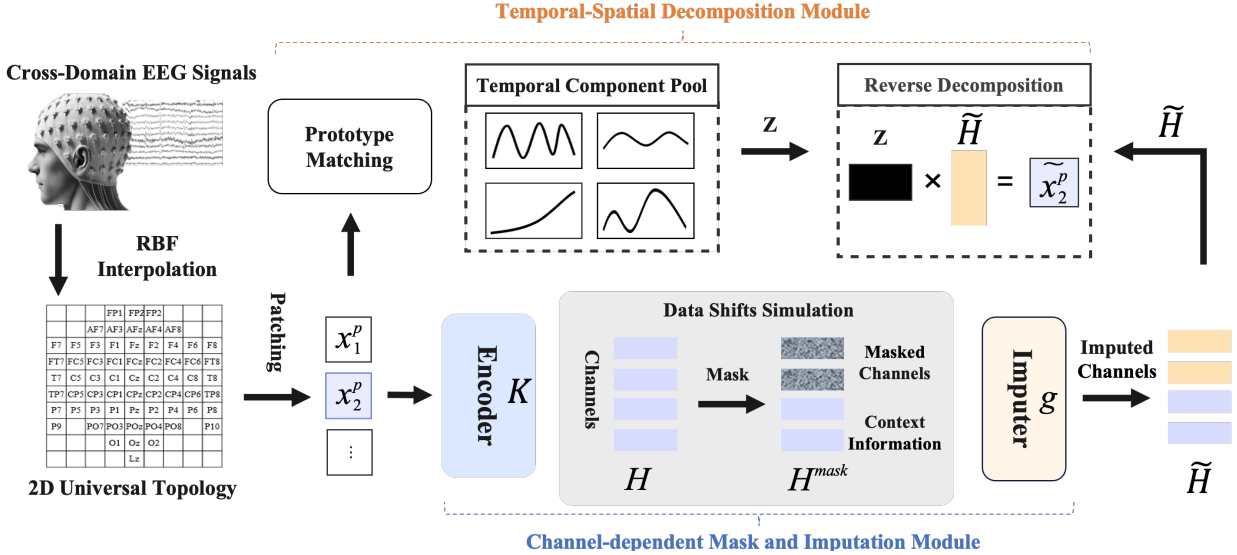


Figure 2: The training procedure of IMAC. The cross-domain EEG signals are first processed through spatial topology unification via RBF Interpolation. These preprocessed patches are then passed through an Encoder f for feature extraction. The extracted features H are randomly masked along the channel dimension and subsequently reconstructed by the imputer module. Simultaneously, each patch of the input signals is decoupled with temporal pattern selection, which is then multiplied with the extracted features to reconstruct the initial EEG data.

each predefined temporal component. The selected component is the one with the highest similarity score:

$$S(\hat{x}^{(p)}) = \arg \max_{k \in \{T, S, R\}} \frac{\hat{x}^{(p)} \cdot Z^k}{\|\hat{x}^{(p)}\| \|Z^k\|}. \quad (1)$$

This selection process ensures that the model utilizes the most appropriate temporal representation based on the specific characteristics of the input signal.

For spatial modeling, the channel correlation matrix H is generated using a channel-dependent encoder \mathcal{K}_θ , which processes the input patch $\hat{x}^{(p)}$ and outputs channel-wise weights as shown in Figure 2. This encoder is implemented as a transformer block with self-attention mechanisms, ensuring that inter-channel dependencies are effectively captured.

Finally, to optimize the temporal-spatial combination, we enforce a reconstruction objective that encourages the model to approximate the original EEG patch by combining the temporal embeddings Z and spatial weights H . The reconstruction loss is defined as:

$$\mathcal{L}_{dec} = \frac{1}{n} \sum_{i=1}^n \| \mathcal{N}(H, Z) - \hat{x}^{(p)} \|^2, \quad (2)$$

where $\mathcal{N}(\cdot, \cdot)$ denotes the matrix multiplication between spatial and temporal factors. This objective ensures that the temporal patterns and spatial weights jointly reconstruct the input signal, promoting better decomposition and alignment under cross-domain variations.

3.3 Channel-dependent Mask and Imputation Module

To address the spatial heterogeneity of EEG signals across different domains, there are prior works suggest that directly modifying

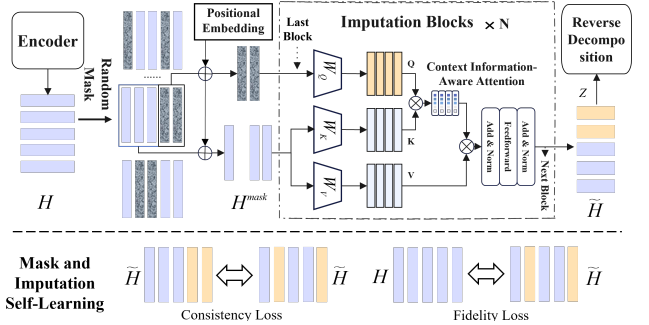


Figure 3: The architecture of the Channel-dependent Mask and Imputation Module.

or correcting the data can be more effective than merely mitigating domain gaps through feature transformation [40]. In line with this, we propose the Channel Masking and Imputation Module. In contrast to existing approaches that focus on low-resolution upsampling [37], CMIM introduces a channel-based masking mechanism and a context-aware imputation strategy to explicitly simulate and recover from cross-domain variability in EEG spatial patterns, as illustrated in Figure 3.

Specifically, CMIM first applies random channel masking to the latent spatial representation $H \in \mathbb{R}^{T' \times d}$, producing a masked version H^{mask} , where certain channels (i.e., rows) are replaced by a shared learnable mask token sampled from a normal distribution:

$$H^{\text{mask}} = (H \odot M) + M_{\text{normal}}, \quad (3)$$

where $M \in \{0, 1\}^{T' \times d}$ is a binary mask matrix indicating masked positions, and \odot denotes element-wise multiplication. M_{normal} represents the randomly sampled placeholder token shared across masked entries.

Next, positional embeddings are added to H^{mask} to encode the spatial ordering of channels. The resulting representation is passed through a stack of imputation blocks, each consisting of a Context Information-Aware Attention module, layer normalization, and feed-forward layers. The attention mechanism is formulated as:

$$\text{Attention}(H^{\text{mask}}, H, H) = \text{softmax} \left(\frac{H^{\text{mask}} W_Q (H W_K)^T}{\sqrt{d_k}} \right) H W_V, \quad (4)$$

where $W_Q, W_K, W_V \in \mathbb{R}^{d \times d_k}$ are learnable projection matrices, and d_k is the attention dimension. Here, masked tokens H^{mask} serve as queries, while the full latent representation H provides the keys and values, allowing reconstruction of missing channels based on global context.

Our architecture employs a multi-layer imputation block design where, starting from the second layer, each block takes the previous layer's output as queries (q) while maintaining consistent keys (k) and values (v) from the original context information throughout all layers. This design preserves the integrity of the contextual information while allowing progressive refinement of the imputed features. The final imputed representations \tilde{H} are obtained as the output of the last layer. For each masked region indexed by $m(i)$, the imputer g_ϕ generates the reconstructed embedding through:

$$\tilde{H}(i) = g_\phi(\text{Attn}_{\text{final}}(q), m(i)), \quad (5)$$

where $\text{Attn}_{\text{final}}(q)$ denotes the output from the final attention layer's query processing, and $m(i)$ encodes the spatial position of the i -th missing segment.

To ensure high-quality imputation and improve generalization across domains, we introduce two complementary learning objectives:

- **Fidelity Loss (\mathcal{L}_{fid}):** Encourages the imputed tokens $\tilde{H}(i)$ to be close to the ground-truth values $H(i)$, promoting accurate recovery:

$$\mathcal{L}_{\text{fid}} = \frac{1}{M} \sum_{i=1}^M \|\tilde{H}(i) - H(i)\|^2. \quad (6)$$

- **Consistency Loss ($\mathcal{L}_{\text{cons}}$):** Measures the discrepancy between imputed results under different random masks applied to the same sample. Let H_n^m and $H_{n'}$ denote different masked versions of the same EEG segment; then:

$$\mathcal{L}_{\text{cons}} = \frac{1}{N} \sum_{n=1}^N \|g_\phi(H_n^m) - g_\phi(H_{n'})\|^2. \quad (7)$$

The total loss combines both terms with a weighting factor λ :

$$\mathcal{L} = \mathcal{L}_{\text{fid}} + \lambda \cdot \mathcal{L}_{\text{cons}}. \quad (8)$$

This dual-objective setup ensures that the imputer produces reliable reconstructions while maintaining consistency across varying masking patterns, thereby enhancing robustness under distribution shifts.

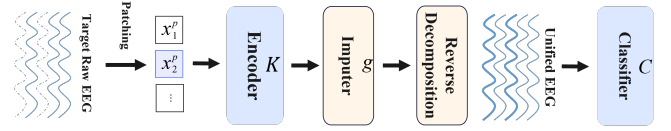


Figure 4: The inference process of the proposed IMAC.

Finally, to prevent noise from imputed channels from negatively impacting downstream classification, the imputation process is integrated as an auxiliary module into the overall IMAC architecture. A classification head C_θ , implemented using EEGNet [13], takes the full reconstructed signal as input and is jointly trained to optimize classification accuracy alongside the imputation loss. This encourages the model to balance between effective feature recovery and discriminative learning, resulting in better cross-domain generalization.

3.4 Model Inference

During inference on target EEG samples as shown in Figure 4, IMAC adopts a deterministic pipeline that omits Spatial Topology Unification and random masking. The process begins by partitioning the raw multichannel EEG signals into spatial-temporal segments $\{x_1^p, x_2^p, \dots\}$, preserving localized signal characteristics. Each segment is then processed through the pretrained encoder K to extract spatial features, followed by the imputer g_ϕ , which deterministically reconstructs missing channels using learned attention patterns.

Subsequently, a reverse decomposition step transforms the features back into signal representations by multiplying them with temporal factors. These domain-invariant features are then fed into the frozen classifier C_θ to generate the final prediction. By eliminating training-time stochasticity, this streamlined pipeline ensures robust handling of unseen channel configurations through stable, learned reconstruction patterns, while maintaining computational efficiency—a critical requirement for real-world deployment.

4 Experiments

4.1 Datasets

In this study, we evaluate IMAC on 10 public EEG datasets covering Parkinson's Disease (PD), motor imagery (MI), and emotion recognition tasks: PD datasets include **UC** (41 ch, 35 subj) [7], **UNM** (64 ch, 42 subj) and **Iowa** (50 ch, 37 subj) [1], and **Finland** (41 ch, 40 subj) [23]. MI datasets include **Cho2017** (32 ch, 52 subj) [2], **PhysionetMI** (64 ch, 109 subj) [24], **BNCI2014001** (22 ch, 10 subj) [31], **Lee2019MI** (62 ch, 54 subj) [14], and **Weibo2014** (30 ch, 10 subj) [42]. Emotion recognition is evaluated on **DEAP** (32 ch, 32 subj) [12].

4.2 Baselines and Implementation Details

To comprehensively evaluate and compare our method with relevant baseline approaches, we select a range of state-of-the-art models. Among these, EEGConformer [26], EEGDeformer [4], Medformer [38], and EEGNet [13] serve as models specifically designed for EEG classification tasks. MCPNet [20], MAPU [22], and POND

Table 1: Cross-Center Results on 4 PD Recognition Datasets and 5 MI Classification Datasets, where each column represents the performance when the corresponding dataset is used as the test set. All values in the table represent Accuracy (%).

Method	Ref	PD Task (Leave-One-Dataset-Out)					MI Task (Leave-One-Dataset-Out)				
		UC	UNM	Iowa	Finland	Avg.	Cho	Physio	BNCI	Lee	Weibo
EEGNet	TNSRE 2023	80.57	78.18	80.69	79.84	79.82	83.37	83.68	83.59	82.85	81.70
EEGConformer	TNSRE 2023	80.43	79.15	80.92	81.02	80.38	84.26	85.33	84.50	85.11	86.75
EEGDeformer	JHBI 2024	81.89	80.26	81.49	82.11	81.44	85.73	86.86	85.95	86.51	87.04
MAPU	KDD 2023	81.12	80.03	80.84	82.15	81.04	85.12	84.43	87.24	86.11	86.95
Medformer	NIPS 2024	82.12	79.53	81.04	82.35	81.26	85.52	85.93	85.44	86.25	86.18
MCPNet	TIM 2024	79.90	81.21	82.01	80.33	80.87	85.39	87.61	87.42	85.02	85.98
POND	KDD 2024	81.08	80.79	82.01	82.51	81.60	88.48	85.79	85.68	85.91	87.81
EEGPT	NeurIPS 2024	79.58	80.61	79.89	80.34	80.11	84.22	84.51	84.20	81.45	84.35
MASER	TNSRE 2024	80.26	80.57	80.38	83.79	81.25	87.26	88.57	86.38	87.69	87.50
SaSDim	IJCAI 2024	82.19	82.20	82.01	83.32	82.41	87.99	87.30	86.11	85.42	85.32
Ours		83.18	84.77	84.91	84.96	84.46	90.23	90.78	91.14	90.96	90.79
Ours		83.18	84.77	84.91	84.96	84.46	90.23	90.78	91.14	90.96	90.79

Table 2: Cross-Center Results on PD Recognition and MI Classification Tasks. The Leave-One-Dataset-Out setting is applied, where each dataset serves as the test set, with the remaining datasets used for training.

Method	PD Task (Leave-One-Dataset-Out)					MI Task (Leave-One-Dataset-Out)				
	Accuracy	F1-score	Precision	Recall	Kappa	Accuracy	F1-score	Precision	Recall	Kappa
EEGNet	79.82 \pm 1.03	79.43 \pm 0.98	79.93 \pm 1.05	79.14 \pm 0.97	63.44 \pm 0.79	82.96 \pm 0.73	82.63 \pm 0.70	83.12 \pm 0.75	82.27 \pm 0.69	66.03 \pm 0.71
EEGConformer	80.38 \pm 1.03	80.32 \pm 1.49	79.26 \pm 1.53	80.21 \pm 1.29	65.22 \pm 0.93	84.26 \pm 1.44	83.47 \pm 1.28	84.35 \pm 1.12	83.25 \pm 1.39	67.11 \pm 0.98
EEGDeformer	81.44 \pm 1.02	81.84 \pm 0.98	81.78 \pm 1.12	81.57 \pm 0.79	66.77 \pm 0.84	86.42 \pm 0.90	86.34 \pm 0.98	85.99 \pm 1.42	86.85 \pm 1.44	68.49 \pm 0.87
MAPU	81.04 \pm 0.93	80.83 \pm 0.89	81.24 \pm 0.95	80.43 \pm 0.88	64.64 \pm 0.71	85.97 \pm 1.10	85.13 \pm 1.05	85.63 \pm 1.12	84.73 \pm 1.04	68.05 \pm 0.88
Medformer	81.26 \pm 1.20	80.97 \pm 1.15	81.53 \pm 1.22	80.63 \pm 1.14	65.01 \pm 0.92	85.95 \pm 0.55	85.63 \pm 0.53	86.17 \pm 0.56	85.23 \pm 0.52	68.63 \pm 0.44
MCPNet	80.87 \pm 0.87	80.91 \pm 0.83	81.35 \pm 0.89	80.53 \pm 0.82	64.82 \pm 0.67	86.48 \pm 1.14	85.34 \pm 1.09	85.73 \pm 1.15	85.02 \pm 1.08	68.24 \pm 0.91
POND	81.60 \pm 0.76	81.03 \pm 0.73	80.47 \pm 0.78	80.93 \pm 0.72	65.12 \pm 0.58	86.73 \pm 1.29	86.03 \pm 1.23	86.53 \pm 1.31	85.63 \pm 1.22	68.94 \pm 1.03
EEGPT	80.11 \pm 0.47	79.83 \pm 0.45	80.42 \pm 0.48	79.31 \pm 0.44	63.84 \pm 0.36	83.75 \pm 1.31	83.83 \pm 1.25	84.31 \pm 1.33	83.24 \pm 1.24	67.32 \pm 1.05
MASER	81.25 \pm 1.53	81.02 \pm 1.46	81.53 \pm 1.55	80.83 \pm 1.45	65.04 \pm 1.17	87.48 \pm 0.63	87.74 \pm 0.60	88.13 \pm 0.64	87.32 \pm 0.59	70.04 \pm 0.50
SaSDim	82.43 \pm 0.49	82.14 \pm 0.47	82.53 \pm 0.50	81.73 \pm 0.46	66.51 \pm 0.38	86.43 \pm 1.16	86.03 \pm 1.11	86.53 \pm 1.18	85.53 \pm 1.10	69.03 \pm 0.93
Ours	84.46\pm0.76	84.13\pm0.73	84.83\pm0.77	83.73\pm0.72	68.82\pm0.58	90.78\pm0.35	90.63\pm0.34	91.03\pm0.36	90.23\pm0.33	72.83\pm0.28

Table 3: Cross-Subject Results on emotion recognition, PD recognition and MI classification task. The Leave-One-Subject-Out setting is applied, where each subject as the test set, with the remaining subjects used for training.

Method	DEAP	UC	Cho	Avg.
EEGNet	69.76	87.88	91.02	82.22
EEGConformer	70.59	86.58	90.81	82.66
EEGDeformer	71.39	87.65	91.34	83.46
Medformer	70.13	86.09	91.76	82.66
MCPNet	71.45	87.92	90.83	83.07
MAPU	71.56	87.99	92.05	83.53
POND	72.23	88.02	92.13	84.13
Ours	73.12	89.11	94.16	85.13

[35] represent cutting-edge domain generalization methods tailored for time series classification. MASER [44] and SaSDim [43]

are advanced spatial time series imputation methods, leveraging unique architectures to enhance spatial resolution and dynamic temporal modeling. EEGPT [34] is a 10-million-parameter pretrained Transformer model capable of extracting effective features from low-resolution EEG signals across diverse domains.

We evaluate the models using accuracy as the primary metric, while also reporting F1-score, precision, recall, and Cohen's kappa as additional indicators under the cross-center experimental setting. To ensure a fair comparison, we reproduce all the methods and conducted experiments under both the Leave-One-Dataset-Out and Leave-One-Subject-Out settings. Specifically, for the Leave-One-Dataset-Out setting in the Parkinson's Disease (PD) task, we select the same 32 channels from the UC San Diego dataset[20], ensuring that each PD dataset consists of 32 channels. We then select one dataset as the test set while using the remaining datasets for training. As shown in Table 1, each column represents the EEG classification results when a specific dataset is used as the test set. For the Motor Imaginary (MI) task, we select 22 channels from the BCNI dataset, ensuring that each MI dataset contains 22 channels.

Beyond cross-dataset evaluation, we also assessed IMAC under a Leave-One-Subject-Out (LOSO) protocol, in which each subject is held out in turn for testing [39]. The results for DEAP, UC, and Cho are shown in Table 3, where each column represents the average performance of all subjects in a particular dataset when used as the test set. In both tables, the "Avg." column indicates the average performance of a method across different datasets under the respective experimental setting.

4.3 Results of Cross-domain EEG Classification

Table 1 displays the accuracy of all methods on each dataset and Table 2 shows the average classification performance in the two tasks under the Leave-One-Dataset-Out settings. Our proposed IMAC consistently outperforms all baselines in both tasks across the 9 cross-center scenarios, demonstrating superior generalization ability under cross-domain data shifts. Specifically, IMAC achieves 84.46% accuracy on the PD recognition task and 90.78% on the MI classification task, representing improvements of 2.03% and 2.30% respectively over the second-best method, MASER. In terms of F1-score, precision, recall, and kappa, IMAC also ranks the highest across both tasks, underscoring its ability to maintain balanced and reliable classification performance.

The most notable performance gain is observed on the BNCI dataset, which is known for its missing channels and inconsistent electrode configurations. As shown in Table 1, our IMAC model achieves an accuracy of 91.14% on the MI task in this challenging scenario, surpassing the second-best method (MASER: 86.38%) by 4.76%. This result suggests that IMAC's channel-aware masking and imputation strategy is particularly effective in mitigating performance degradation caused by severe spatial distortions and non-uniform sensor setups. Among the baselines, SaSDim and MASER show the strongest results overall. SaSDim achieves the second-best performance on the PD task with 82.43% accuracy, while MASER ranks second on the MI task with 87.48%. Nonetheless, these methods still trail behind IMAC across all metrics, particularly under high-variance and low-resolution conditions, which are exacerbated in cross-center evaluations.

Although large-scale brain models like EEGPT have demonstrated strong capabilities in extracting cross-domain EEG features, their performance under cross-center settings remains suboptimal. As shown in Table 2, EEGPT achieves 80.11% accuracy on the PD task and 83.75% on the MI task—significantly lower than the results achieved by our proposed IMAC framework. In addition, the EEGNet classifier yields the poorest performance under real-world domain shifts, further underscoring the limitations of conventional models in handling complex distribution discrepancies. These findings highlight that strong feature extraction alone is insufficient; without effective spatio-temporal alignment at the signal level, such models struggle to cope with practical deployment challenges—particularly those involving severe variations in sensor locations and heterogeneous electrode configurations.

Table 3 presents the results of the Leave-One-Subject-Out experiments for emotion recognition, PD recognition, and MI classification tasks. In comparison with the results in Table 1, domain generalization methods like MCPNet, MAPU and POND demonstrate strong performance. Specifically, the second-performing method

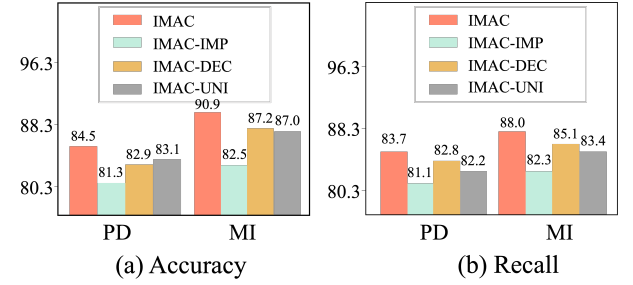


Figure 5: Ablation study performance comparison between IMAC and three variant models on two EEG classification tasks.

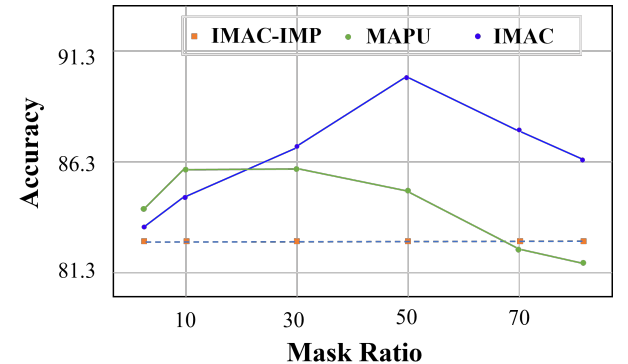


Figure 6: Analysis of adaptation performance with varying mask ratio for self-supervised learning methods. The blue, green and yellow points represent the accuracy results from IMAC, MAPU and IMAC-IMP, respectively.

POND achieves 84.13%, indicating their effectiveness in capturing domain-invariant information when addressing temporal variability in cross-subject scenarios. While our proposed method maintains a consistent advantage across all three tasks, achieving an overall average accuracy of 85.13%, which is 1% higher than the second-best method, POND. Moreover, on challenging tasks such as emotion recognition, our IMAC performs the best accuracy of 73.12%, excelling by 0.89% than the second performing POND, emphasizing the robustness of our method in handling domain shifts caused by subject-specific variations.

4.4 Ablation Study

To evaluate the contribution of each module in IMAC for addressing real-world data shift problems, we conducted an ablation study comparing IMAC with three variants. **IMAC-IMP** retains only the matrix factorization module. **IMAC-DEC** is a version of IMAC without the matrix factorization module. **IMAC-UNI** removes the spatial topology unification module. The challenging Leave-One-Dataset-Out setting is utilized to test the performance.

Figure 5 presents the accuracy and recall performance of these variants compared to the full IMAC model. Overall, IMAC achieves

the best performance when all three modules are present, underscoring their necessity for handling real-world data shifts effectively. Notably, the largest performance drop is observed in the MI task. IMAC achieves an accuracy of 90.9%, while IMAC-IMP only reaches 82.5%, resulting in a significant accuracy decline of 8.4%. This highlights the challenges posed by the inherent data shifts in MI tasks, which are characterized by substantial differences in EEG collection paradigms. Without the Channel-dependent Mask and Imputation Module, IMAC-IMP fails to capture a unified topology, leading to decreased classification accuracy.

Among the variants, IMAC-IMP performs the worst across all scenarios, with a 3% to 8% drop in both accuracy and recall for both tasks. This is because it relies solely on spatial correlations between electrode locations, neglecting the spatial alignment of EEG signals. Both IMAC-DEC and IMAC-UNI exhibit better performance than IMAC-IMP but still lag behind the full IMAC model. IMAC-DEC applies the encoder \mathcal{K}_θ directly for temporal-spatial feature extraction, while IMAC-UNI operates on EEG signals with fewer channels, omitting spatial topology unification. These variants show a 2% reduction in accuracy and recall in the PD task and a 4% reduction in the MI task compared to IMAC.

The masking ratio during self-supervised pretraining is crucial, as it defines the balance between task difficulty and representation quality. Further, to explore how IMAC performs under varying levels of missing data, we evaluate its accuracy at six specific masking ratios: 5%, 10%, 30%, 50%, 70%, and 80%. As shown in Figure 6, IMAC’s performance improves as the mask ratio increases, peaking at 50%, before declining at higher ratios. This indicates that moderate masking enables IMAC to better exploit its cross-channel imputation mechanism, while excessive masking reduces available context and hampers reconstruction quality. Notably, even at extreme ratios such as 80%, IMAC still outperforms the baseline without imputation, demonstrating its robustness.

To further assess imputation strategies under varying degrees of missing information, we include MAPU as a comparison method. MAPU exhibits a contrasting trend: its performance remains relatively stable across different mask ratios, with only slight fluctuations. This suggests that MAPU’s design may limit its sensitivity to increased masking, potentially due to a lack of adaptive spatial modeling. Compared with IMAC, MAPU performs competitively at low mask ratios (e.g., 5%, 10%) but fails to scale effectively as the imputation challenge intensifies. The comparison underscores IMAC’s superior capacity for learning informative representations from partially observed EEG data, especially when large portions of the input are missing.

4.5 Signal Integrity Measurement in Real-world Simulation

Although our experiments on 10 datasets already highlight the superior performance of IMAC under real-world data variability, we further evaluate its generalizability in simulated real-world data shifts during actual deployment. Following the study of [33], we simulate real-world data shifts by introducing noise and variability inherent in diverse datasets and emulate the data acquisition process across different devices by altering data characteristics.

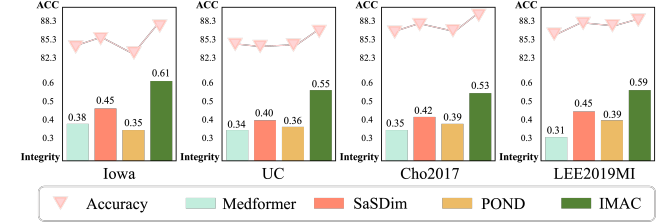


Figure 7: Analysis of simulated real-world data shifts on IMAC, Medformer, SaSDim, and POND across four datasets.

The following three types of data shifts were applied to different individuals within the same dataset:

- Application of a (1-25 Hz) band-pass filter;
- Addition of broadband or narrowband noise ($\sigma = 0.1$);
- Implementation of a 50% channel mask.

We measure the integrity of extracted features in the more challenging cross-center deployment using Delaunay neighborhood graphs, and compare classification results with well-performed Medformer, SaSDim, POND, and the proposed IMAC on the modified and unmodified versions of the LEE2019MI, UC, Cho2017, and Iowa datasets. As shown in Figure 7, IMAC consistently outperforms the comparison methods in terms of integrity across all four datasets. Specifically, IMAC achieves the highest integrity scores on the modified versions of the Iowa, UC, Cho2017, and LEE2019MI datasets, demonstrating its robustness to real-world data shifts and noise. IMAC outperforms Medformer and POND by up to 35%~74% in integrity, with the largest performance gap observed on the Iowa dataset, where IMAC achieves an integrity score of 0.61, compared to SaSDim’s 0.45 and Medformer’s 0.38. This improvement highlights the effectiveness of IMAC in maintaining feature integrity under challenging real-world conditions.

5 Conclusion

In this paper, we introduce IMAC, a novel framework designed to tackle the challenges of cross-domain data shifts in EEG classification. By applying channel masking to simulate domain shifts, IMAC enables cross-domain knowledge transfer and learns to reconstruct consistent signal representations through a spatial imputation process. Extensive experiments on 10 EEG classification datasets including emotion recognition, Parkinson’s disease detection, and motor imagery tasks, demonstrating that IMAC consistently outperforms state-of-the-art methods. The effectiveness of IMAC highlights the potential of incorporating spatial imputation to address a wide array of adaptation challenges.

Acknowledgments

This work was supported by the National Key Research and Development Program of China (Grant No. 2022ZD0118001), the National Natural Science Foundation of China (Grant Nos. U22A2022, 62332017), and was conducted in part at the MOE Key Laboratory of Advanced Materials and Devices for Post-Moore Chips, the Beijing Key Laboratory of Big Data Innovation and Application for Skeletal Health Medical Care, and the Beijing Advanced Innovation Center for Materials Genome Engineering.

References

- [1] Md Fahim Anjum, Soura Dasgupta, Raghuraman Mudumbai, Arun Singh, James F Cavanagh, and Nandakumar S Narayanan. 2020. Linear Predictive Coding Distinguishes Spectral EEG Features of Parkinson's Disease. *Parkinsonism & Related Disorders* 79 (2020), 79–85.
- [2] Hohyun Cho, Minkyu Ahn, Sangtae Ahn, Moonyoung Kwon, and Sung Chan Jun. 2017. EEG Datasets for Motor Imagery Brain–Computer Interface. *GigaScience* 6, 7 (2017), gix034.
- [3] Hristos S Courellis, John R Iversen, Howard Poizner, and Gert Cauwenberghs. 2016. EEG Channel Interpolation Using Ellipsoid Geodesic Length. In *2016 IEEE Biomedical Circuits and Systems Conference*. IEEE, 540–543.
- [4] Yi Ding, Yong Li, Hao Sun, Rui Liu, Chengxuan Tong, Chenyu Liu, Xinliang Zhou, and Cuntai Guan. 2025. EEG-Deformer: A Dense Convolutional Transformer for Brain–Computer Interfaces. *IEEE Journal of Biomedical and Health Informatics* 29, 3 (2025), 1909–1918. doi:10.1109/JBHI.2024.3504604
- [5] Yi Ding, Neethu Robinson, Su Zhang, Qiuhan Zeng, and Cuntai Guan. 2023. TSeption: Capturing Temporal Dynamics and Spatial Asymmetry From EEG for Emotion Recognition. *IEEE Transactions on Affective Computing* 14, 3 (2023), 2238–2250. doi:10.1109/TAFFC.2022.3169001
- [6] Wengui Huang, Guanghui Yan, Wenwen Chang, Yuchan Zhang, and Yuetong Yuan. 2023. EEG-Based Classification Combining Bayesian Convolutional Neural Networks with Recurrence Plot for Motor Movement/Imagery. *Pattern Recognition* 144 (2023), 109838. doi:10.1016/j.patcog.2023.109838
- [7] Nicko Jackson, Scott R Cole, Bradley Voytek, and Nicole C Swann. 2019. Characteristics of Waveform Shape in Parkinson's Disease Detected with Scalp Electroneurography. *Eneuro* 6, 3 (2019).
- [8] H. Jasper. 1958. The Ten-twenty Electrode System of the International Federation. *Electroencephalography and Clinical Neurophysiology* 10, 2 (1958), 371–375.
- [9] Ziyu Jia, Youfang Lin, Jing Wang, Xiaojun Ning, Yuanlai He, Ronghao Zhou, Yuhua Zhou, and H Lehman Li-wei. 2021. Multi-view Spatial-temporal Graph Convolutional Networks with Domain Generalization for Sleep Stage Classification. *IEEE Transactions on Neural Systems and Rehabilitation Engineering* 29 (2021), 1977–1986.
- [10] Weibang Jiang, Liming Zhao, and Bao-liang Lu. 2024. Large Brain Model for Learning Generic Representations with Tremendous EEG Data in BCI. In *The Twelfth International Conference on Learning Representations*.
- [11] Shuo Jin, Meiqin Liu, Chao Yao, Chunyu Lin, and Yao Zhao. 2023. Kernel Dimension Matters: To Activate Available Kernels for Real-Time Video Super-Resolution. In *Proceedings of the 31st ACM International Conference on Multimedia*. Association for Computing Machinery, New York, NY, USA, 8617–8625. doi:10.1145/3581783.3611908
- [12] Sander Koelstra, Christian Muhl, Mohammad Soleymani, Jong-Seok Lee, Ashkan Yazdani, Touradj Ebrahimi, Thierry Pun, Anton Nijholt, and Ioannis Patras. 2012. DEAP: A Database for Emotion Analysis Using Physiological Signals. *IEEE Transactions on Affective Computing* 3, 1 (2012), 18–31. doi:10.1109/T-AFFC.2011.15
- [13] Vernon J Lawhern, Amelia J Solon, Nicholas R Waytowich, Stephen M Gordon, Chou P Hung, and Brent J Lance. 2018. EEGNet: A Compact Convolutional Neural Network for EEG-Based Brain–Computer Interfaces. *Journal of Neural Engineering* 15, 5 (2018), 056013.
- [14] Min-Ho Lee, O-Yeon Kwon, Yong-Jeong Kim, Hong-Kyung Kim, Young-Eun Lee, John Williamson, Siamac Fazli, and Seong-Whan Lee. 2019. EEG dataset and OpenBMI toolbox for three BCI paradigms: An investigation into BCI illiteracy. *GigaScience* 8, 5 (2019), giz002.
- [15] Dongdong Li, Zhongliang Zeng, Zhe Wang, and Hai Yang. 2025. ESTformer: Transformer utilizing spatiotemporal dependencies for electroencephalogram super-resolution. *Knowledge-Based Systems* (2025), 113345. doi:10.1016/j.knosys.2025.113345
- [16] Shuang Liang, Changsheng Xuan, Wenlong Hang, Baiying Lei, Jun Wang, Jing Qin, Kup-Sze Choi, and Yu Zhang. 2023. Domain-Generalized EEG Classification With Category-Oriented Feature Decorrelation and Cross-View Consistency Learning. *IEEE Transactions on Neural Systems and Rehabilitation Engineering* 31 (2023), 3285–3296. doi:10.1109/TNSRE.2023.3300961
- [17] Meiqin Liu, Shuo Jin, Chao Yao, Chunyu Lin, and Yao Zhao. 2023. Temporal Consistency Learning of Inter-Frames for Video Super-Resolution. *IEEE Transactions on Circuits and Systems for Video Technology* 33, 4 (2023), 1507–1520.
- [18] Meiqin Liu, Chenming Xu, Chao Yao, Chunyu Lin, and Yao Zhao. 2023. JNMR: Joint Non-Linear Motion Regression for Video Frame Interpolation. *IEEE Transactions on Image Processing* 32 (2023), 5283–5295.
- [19] Sara Petrichella, L Vollere, Florinda Ferreri, Andrea Guerra, S Määttä, Mervi Kõnnönen, Vincenzo Di Lazzaro, and Giulio Iannello. 2016. Channel Interpolation in TMS-EEG: A Quantitative Study towards An Accurate Topographical Representation. In *2016 38th Annual International Conference of the IEEE Engineering in Medicine and Biology Society*. IEEE, 989–992.
- [20] Lina Qiu, Jianping Li, Liangquan Zhong, Weisen Feng, Chengju Zhou, and Jiahui Pan. 2024. A Novel EEG-Based Parkinson's Disease Detection Model Using Multiscale Convolutional Prototype Networks. *IEEE Transactions on Instrumentation and Measurement* (2024).
- [21] Mohamed Ragab, Emaddeen Eldele, Zhenghua Chen, Min Wu, Chee-Keong Kwoh, and Xiaoli Li. 2024. Self-Supervised Autoregressive Domain Adaptation for Time Series Data. *IEEE Transactions on Neural Networks and Learning Systems* 35, 1 (2024), 1341–1351. doi:10.1109/TNNLS.2022.3183252
- [22] Mohamed Ragab, Emaddeen Eldele, Min Wu, Chuan-Sheng Foo, Xiaoli Li, and Zhenghua Chen. 2023. Source-free Domain Adaptation with Temporal Imputation for Time Series Data. In *Proceedings of the 29th ACM SIGKDD Conference on Knowledge Discovery and Data Mining*. 1989–1998.
- [23] Henry Railo, Niklas Nokelainen, Saara Savolainen, and Valterti Kaasinen. 2020. Deficits in Monitoring Self-produced Speech in Parkinson's Disease. *Clinical Neurophysiology* 131, 9 (2020), 2140–2147.
- [24] Gerwin Schalk, Dennis J McFarland, Thilo Hinterberger, Niels Birbaumer, and Jonathan R Wolpaw. 2004. BCI2000: A General-purpose Brain-computer Interface (BCI) System. *IEEE Transactions on biomedical engineering* 51, 6 (2004), 1034–1043.
- [25] Qingshan She, Tie Chen, Feng Fang, Jianhai Zhang, Yunyan Gao, and Yingchun Zhang. 2023. Improved Domain Adaptation Network based on Wasserstein Distance for Motor Imagery EEG Classification. *IEEE Transactions on Neural Systems and Rehabilitation Engineering* 31 (2023), 1137–1148.
- [26] Yonghao Song, Qingqing Zheng, Bingchuan Liu, and Xiaorong Gao. 2023. EEG Conformer: Convolutional Transformer for EEG Decoding and Visualization. *IEEE Transactions on Neural Systems and Rehabilitation Engineering* 31 (2023), 710–719. doi:10.1109/TNSRE.2022.3230250
- [27] Yuxiao Sun, Yao Zhao, Meiqin Liu, Chao Yao, Huihui Bai, Chunyu Lin, and Weisi Lin. 2025. TransVFC: A Transformable Video Feature Compression Framework for Machines. *Pattern Recognition* (2025), 112091.
- [28] Qi Tang, Yao Zhao, Meiqin Liu, Jian Jin, and Chao Yao. 2024. Semantic Lens: Instance-Centric Semantic Alignment for Video Super-resolution. In *Proceedings of the AAAI Conference on Artificial Intelligence*, Vol. 38, 5154–5161.
- [29] Qi Tang, Yao Zhao, Meiqin Liu, and Chao Yao. 2024. SeeClear: Semantic Distillation Enhances Pixel Condensation for Video Super-resolution. *Advances in Neural Information Processing Systems* 37 (2024), 134902–134926.
- [30] Yunbo Tang, Dan Chen, Honghai Liu, Chang Cai, and Xiaoli Li. 2023. Deep EEG Superresolution via Correlating Brain Structural and Functional Connectivities. *IEEE Transactions on Cybernetics* 53, 7 (2023), 4410–4422. doi:10.1109/TCYB.2022.3178370
- [31] Michael Tangermann, Klaus-Robert Müller, Ad Aertsen, Niels Birbaumer, Christoph Braun, Clemens Brunner, Robert Leeb, Carsten Mehring, Kai J Müller, Gernot R Müller-Putz, et al. 2012. Review of the BCI Competition IV. *Frontiers in Neuroscience* 6 (2012), 55.
- [32] Maximilian Toller, Tiago Santos, and Roman Kern. 2019. SAZED: Parameter-free Domain-agnostic Season Length Estimation in Time Series Data. *Data Mining and Knowledge Discovery* 33, 6 (2019), 1775–1798.
- [33] Neeraj Wagh, Jionghao Wei, Samarth Rawal, Brent M Berry, and Yogatheeasan Varatharajah. 2022. Evaluating Latent Space Robustness and Uncertainty of EEG-ML Models under Realistic Distribution Shifts. *Advances in Neural Information Processing Systems* 35 (2022), 21142–21156.
- [34] Guangyu Wang, Wenchaoyi Liu, Yuhong He, Cong Xu, Lin Ma, and Haifeng Li. 2024. EEGPT: Pretrained Transformer for Universal and Reliable Representation of EEG Signals. In *Advances in Neural Information Processing Systems*, Vol. 37. Curran Associates, Inc., 39249–39280. https://proceedings.neurips.cc/paper_files/paper/2024/file/4540d267eeec4e5dbd9dae9448f0b739-Paper-Conference.pdf
- [35] Junxiang Wang, Guangji Bai, Wei Cheng, Zhengzhang Chen, Liang Zhao, and Haifeng Chen. 2023. POND: Multi-Source Time Series Domain Adaptation with Information-Aware Prompt Tuning. In *the 30th ACM SIGKDD Conference on Knowledge Discovery and Data Mining*.
- [36] Jindong Wang, Cuiling Lan, Chang Liu, Yidong Ouyang, Tao Qin, Wang Lu, Yiqiang Chen, Wenjun Zeng, and Philip S Yu. 2023. Generalizing to Unseen Domains: A Survey on Domain Generalization. *IEEE Transactions on Knowledge and Data Engineering* 35, 8 (2023), 8052–8072. doi:10.1109/TKDE.2022.3178128
- [37] Shuqiang Wang, Tong Zhou, Yanyan Shen, Ye Li, Guoheng Huang, and Yong Hu. 2025. Generative AI Enables EEG Super-Resolution via Spatio-Temporal Adaptive Diffusion Learning. *IEEE Transactions on Consumer Electronics* 71, 1 (2025), 1034–1045. doi:10.1109/TCE.2025.3528438
- [38] Yifei Wang, Nan Huang, Taida Li, Yujun Yan, and Xiang Zhang. 2024. Medformer: A Multi-Granularity Patching Transformer for Medical Time-Series Classification. *Advances in Neural Information Processing Systems* (2024).
- [39] Yiming Wang, Bin Zhang, and Yuqiao Tang. 2024. DMMR: Cross-Subject Domain Generalization for EEG-Based Emotion Recognition via Denoising Mixed Mutual Reconstruction. In *Proceedings of the AAAI Conference on Artificial Intelligence*, Vol. 38, 628–636.
- [40] Ziwei Wang, Siyang Li, and Dongrui Wu. 2025. Canine EEG Helps Human: Cross-Species and Cross-Modality Epileptic Seizure Detection via Multi-space Alignment. *National Science Review* (03 2025), nwaf086. doi:10.1093/nsr/nwaf086
- [41] Dong-qin Xu and Ming-ai Li. 2023. A Dual Alignment-Based Multi-Source Domain Adaptation Framework for Motor Imagery EEG Classification. *Applied Intelligence* 53, 9 (2023), 10766–10788.
- [42] Weibo Yi, Shuang Qiu, Kun Wang, Hongzhi Qi, Lixin Zhang, Peng Zhou, Feng He, and Dong Ming. 2014. Evaluation of EEG Oscillatory Patterns and Cognitive

- Process during Simple and Compound Limb Motor Imagery. *PLoS One* 9, 12 (2014), e114853.
- [43] Shunyang Zhang, Senzhang Wang, Xianzhen Tan, Renzhi Wang, Ruochen Liu, Jian Zhang, and Jianxin Wang. 2024. SaSDim: Self-Adaptive Noise Scaling Diffusion Model for Spatial Time Series Imputation. In *Proceedings of the Thirty-Third International Joint Conference on Artificial Intelligence*. International Joint Conferences on Artificial Intelligence Organization, 2561–2569.
- doi:10.24963/ijcai.2024/283
- [44] Yifan Zhang, Yang Yu, Hao Li, Anqi Wu, Ling-Li Zeng, and Dewen Hu. 2024. MASER: Enhancing EEG Spatial Resolution With State Space Modeling. *IEEE Transactions on Neural Systems and Rehabilitation Engineering* 32 (2024), 3858–3868. doi:10.1109/TNSRE.2024.3481886